# Dynamical excitation of maxon and roton modes in a Rydberg-dressed Bose-Einstein condensate

Gary McCormack,[1,*] Rejish Nath,[2] and Weibin Li[1]

[1]*School of Physics and Astronomy, and Centre for the Mathematics and Theoretical Physics of Quantum Non-Equilibrium Systems, University of Nottingham, Nottingham NG7 2RD, United kingdom*

[2]*Indian Institute of Science Education and Research, Pune 411008, India*

(Received 28 February 2020; accepted 14 July 2020; published 19 August 2020)

We investigate the dynamics of a three-dimensional Bose-Einstein condensate of ultracold atomic gases with a soft-core-shaped long-range interaction, which is induced by laser dressing the atoms to a highly excited Rydberg state. For a homogeneous condensate, the long-range interaction drastically alters the dispersion relation of the excitation, supporting both roton and maxon modes. Rotons are typically responsible for the creation of supersolids, while maxons are normally dynamically unstable in BECs with dipolar interactions. We show that maxon modes in the Rydberg-dressed condensate, on the contrary, are dynamically stable. We find that the maxon modes can be excited through an interaction quench, i.e., turning on the soft-core interaction instantaneously. The emergence of the maxon modes is accompanied by oscillations at high frequencies in the quantum depletion, while rotons lead to much slower oscillations. The dynamically stable excitation of the roton and maxon modes leads to persistent oscillations in the quantum depletion. Through a self-consistent Bogoliubov approach, we identify the dependence of the maxon mode on the soft-core interaction. Our study shows that maxon and roton modes can be excited dynamically and simultaneously by quenching Rydberg-dressed long-range interactions. This is relevant to current studies in creating and probing exotic states of matter with ultracold atomic gases.

DOI: 10.1103/PhysRevA.102.023319

## I. INTRODUCTION

Collective excitations induced by particle-particle interactions play an important role in the understanding of static and dynamical properties of many-body systems. The ability to routinely create and precisely control properties of ultracold atomic gases opens exciting prospects to manipulate and probe collective excitations. In weakly interacting Bose-Einstein condensates (BECs) with *s*-wave interactions [1–4], phonon excitations reduce the condensate density, giving rise to *quantum depletion* [5]. It has been shown [6] that quantum depletion can be enhanced by increasing the *s*-wave scattering length through Feshbach resonances [7,8]. By dynamically changing the *s*-wave scattering length [9], phonon excitations can alter the quantum depletion, momentum distribution [10], correlations [11], contact [12,13], and statistics [14] of the condensate. Moreover, phonon-induced quantum depletion plays a vital role in the formation of droplets in BECs [15].

When long-range interactions are introduced, the dispersion relation corresponding to the quasiparticle spectrum of a BEC is qualitatively different, where the excitation energies of the collective modes depend nonmonotonically on the momentum. Previously BECs with dipole-dipole interactions have been extensively examined [16–22]. In two-dimensional (2D) dipolar BECs [23], *roton* and *maxon* modes emerge, with roton (maxon) modes corresponding to local minima (maxima) in the dispersion relation. The strength of dipolar interactions can be tuned by either external electric or magnetic fields [19]. When instabilities of roton modes are triggered, a homogeneous BEC undergoes density modulations such that a supersolid phase could form. The existence of roton modes has been supported by a recent experiment of ultracold dipolar gases [24]. Maxon modes, on the other hand, normally appear at lower-momentum states [23]. It was shown, however, that the maxon modes in dipolar BECs are typically unstable and decay rapidly through Beliaev damping [20,21].

Strong and long-range interactions are also found in gases of ultracold Rydberg atoms [25–29]. Rydberg atoms are in highly excited electronic states and interact via long-range van der Waals (vdW) interactions. The strength of the vdW interaction is proportional to $\mathcal{N}^{11}$, with $\mathcal{N}$ being the principal quantum number in the Rydberg state. For large $\mathcal{N}$ (current experiments exploit $\mathcal{N}$ typically between 30 and 100), the interaction between two Rydberg atoms can be as large as several megahertz at a separation of several micrometers [30]. However, lifetimes in Rydberg states are typically 10–100 $\mu$s, which is not long enough to explore spatial coherence. As a result, *Rydberg dressing*, in which a far-detuned laser couples electronic ground states to Rydberg states, is proposed. The laser coupling generates a long-range, *soft-core* type interaction between Rydberg-dressed atoms [31–41]. The coherence time and interaction strength can be controlled by the dressing laser [35]. With this dressed interaction, interesting physics, such as magnets [42], transport [43], supersolids [31,34,44,45], etc., have been studied. Signatures of the dressed interaction have been experimentally demonstrated with atoms trapped in optical lattices and optical tweezers [42,46].

In this paper, we study excitations of roton and maxon modes in three-dimensional (3D) Rydberg-dressed BECs in free space at zero temperature. Three-dimensional uniform

*gary.mccormack@nottingham.ac.uk

 

trapping potentials of ultracold atoms have been realized experimentally [47]. When the soft-core interaction is strong, both the roton and the maxon modes are found in the dispersion relation of the collective excitations. Starting from a weakly interacting BEC, roton and maxon modes are dynamically excited by instantaneously switching on the Rydberg-dressed interaction. Through a self-consistent Bogoliubov calculation, we show that the roton and maxon modes lead to nonequilibrium dynamics, where the quantum depletion exhibits slow and fast oscillations. Through analyzing the Bogoliubov spectra, we identify that the slow oscillations correspond to the excitation of the roton modes, while the fast oscillations come from the excitation of the maxon modes. The dependence these modes have on the quantum depletion in the long-time limit is determined analytically and numerically.

The paper is organized as follows. In Sec. II, the Hamiltonian of the system and properties of the soft-core interaction are introduced. Bogoliubov methods, which are capable of studying static as well as dynamics of the excitation, are presented. In Sec. III, dispersion relations are found using the static Bogoliubov calculation, where roton and maxon modes are identified. We then examine the dynamics of the quantum depletion due to the interaction quench. Excitations of the roton and maxon modes are studied using a self-consistent Bogoliubov method. The asymptotic behavior of the BEC at long times is also explored. Finally, in Sec. IV we conclude our work.

## II. HAMILTONIAN AND METHOD

### A. Hamiltonian of the Rydberg-dressed BEC

We consider a uniform 3D Bose gas of $N$ atoms that interact through both $s$-wave and soft-core interactions. The Hamiltonian of the system is given by ($\hbar \equiv 1$)

$$\hat{H} = \int \psi^\dagger(\mathbf{r})\left(-\frac{\nabla^2}{2m} - \mu\right)\psi(\mathbf{r})\,d\mathbf{r} + \frac{1}{2}\int \psi^\dagger(\mathbf{r})\psi^\dagger(\mathbf{r}')\tilde{g}(\mathbf{r}-\mathbf{r}')\psi(\mathbf{r})\psi(\mathbf{r}')\,d\mathbf{r}\,d\mathbf{r}', \quad (1)$$

where $\psi(\mathbf{r})$ is the annihilation operator of the bosonic field, $\mu$ is the chemical potential, $m$ is the mass of a boson, and $\nabla$ is the 3D nabla operator on coordinate $\mathbf{r} = \{x, y, z\}$. The interaction potential is described by $\tilde{g}(\mathbf{r}-\mathbf{r}') = g_0\delta(\mathbf{r}) + \tilde{V}(\mathbf{r}-\mathbf{r}')$, where $g_0 = 4\pi a_s/m$ is the short-range contact interaction controlled by the $s$-wave scattering length $a_s$ [3]. $\tilde{V}(\mathbf{r}-\mathbf{r}')$ is the long-range soft-core interaction,

$$\tilde{V}(\mathbf{r}-\mathbf{r}') = \frac{C_0}{R^6 + |\mathbf{r}-\mathbf{r}'|^6}, \quad (2)$$

where $C_0$ is the strength of the dressed interaction potential and $R$ is the soft-core radius [35]. Both these parameters can be tuned independently by varying the dressing laser [35]. The interaction potential saturates to a constant, i.e., $\tilde{V}(\mathbf{r}) \to C_0/R^6$ when $|\mathbf{r}| \ll R$, and approaches a vdW type at distances of $|\mathbf{r}| \gg R$, i.e., $\tilde{V}(\mathbf{r}) \to C_0/|\mathbf{r}|^6$. An example of the soft-core potential is shown in Fig. 1(a). The Fourier transformation of the soft-core potential is $V(k) = U_0 f(k)$, where $U_0 = C_0/R^6$

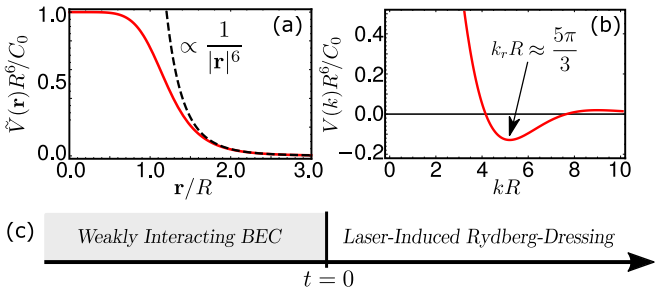


FIG. 1. Soft-core interaction and quench scheme. (a) The soft-core interaction as a function of the interatomic distance $\mathbf{r}$. The energy is scaled by $R^6/C_0$, with $R$ and $C_0$ the soft-core radius and dispersion coefficient. The interaction is constant when $\mathbf{r} \ll R$ and becomes a vdW type when $\mathbf{r} \gg R$. (b) Fourier transformation of the soft-core interaction. The minimum of the interaction is located at $k_rR \approx 5\pi/3$, where the interaction is attractive. (c) The quench scheme. A weakly interacting BEC with $s$-wave interactions is first prepared. The laser dressing is applied at $t > 0$, which induces the soft-core interaction.

determines the strength and $f(k)$ has an analytical form,

$$f(k) = \frac{2\pi^2 e^{-\frac{kR}{2}}}{3kR}\left[e^{-\frac{kR}{2}} - 2\sin\left(\frac{\pi}{6} - \frac{\sqrt{3}kR}{2}\right)\right],$$

which characterizes the momentum dependence of the interaction. Though the interaction is repulsive in real space, i.e., $\tilde{V}(\mathbf{r}) > 0$, it contains negative regions in momentum space, as shown in Fig. 1(b). The negative part of $V(k)$ appears at a momentum around $kR \sim 5\pi/3$. Previously, it was shown that the attractive interaction is crucially important to the formation of roton instabilities, as revealed by the Bogoliubov approximation [23].

### B. Time-independent Bogoliubov approach

In momentum space, we expand the field operators using a plane-wave basis, $\psi(\mathbf{r}) = 1/\sqrt{\Omega}\sum_{\mathbf{k}} e^{i\mathbf{k}\cdot\mathbf{r}}\hat{a}_{\mathbf{k}}$. The many-body Hamiltonian can be rewritten as

$$\hat{H} = \sum_{\mathbf{k}}(\epsilon_k - \mu)\hat{a}^\dagger_{\mathbf{k}}\hat{a}_{\mathbf{k}} + \sum_{\mathbf{q},\mathbf{k},\mathbf{k}'}\frac{g_k}{2\Omega}\hat{a}^\dagger_{\mathbf{k}+\mathbf{q}}\hat{a}^\dagger_{\mathbf{k}'-\mathbf{q}}\hat{a}_{\mathbf{k}}\hat{a}_{\mathbf{k}'}, \quad (3)$$

where $\hat{a}^\dagger_{\mathbf{k}}$ ($\hat{a}_{\mathbf{k}}$) is the creation (annihilation) operator of the momentum state $\mathbf{k}$, and $\Omega$ the volume of the BEC. The kinetic energy is $\epsilon_k = k^2/2m$ with $k = |\mathbf{k}|$, while the Fourier transformation of the atomic interaction $\tilde{g}(\mathbf{r}-\mathbf{r}')$ is given by $g_k = g_0 + V(k)$.

For a homogeneous condensate and in the stationary regime, we apply a conventional Bogoliubov approach [48,49] to study the excitation spectra. At zero temperature we assume a macroscopic occupation in the condensate, which allows us to replace $\hat{a}_0 \approx \sqrt{N_0}$, with $N_0$ being the number of condensed atoms. We then apply a canonical transformation on the bosonic operators of the nonzero momentum states [3], $\hat{a}_{\mathbf{k}\neq 0} = \bar{u}_k\hat{b}_{\mathbf{k}} - \bar{v}^*_k\hat{b}^\dagger_{-\mathbf{k}}$, where $b_{\mathbf{k}}$ ($\hat{b}^\dagger_{-\mathbf{k}}$) is the annihilation (creation) operator for bosonic quasiparticles and $\bar{u}_k$ and $\bar{v}_k$ are complex numbers such that $|\bar{u}_k|^2 - |\bar{v}_k|^2 = 1$, which satisfies the bosonic commutation relation [3]. The excitation spectra of the Bogoliubov modes for different momentum

components give the dispersion relation,

$$\bar{E}_k = \sqrt{\epsilon_k[\epsilon_k + 2g_k n_0]}, \tag{4}$$

with $n_0 = N_0/\Omega$ being the density of the condensed atoms. The coefficients in the Bogoliubov transformation are [3]

$$\bar{u}_k = \sqrt{\frac{1}{2}\left[\frac{\epsilon_k + g_k n_0}{\bar{E}_k} + 1\right]},$$
$$\bar{v}_k = -\sqrt{\frac{1}{2}\left[\frac{\epsilon_k + g_k n_0}{\bar{E}_k} - 1\right]}. \tag{5}$$

The distribution of the noncondensed atoms is given by $n_k = \langle a_k^\dagger a_k\rangle = |\bar{v}_k|^2$. Taking into account contributions from all noncondensed components, the quantum depletion in the stationary state is evaluated as $\bar{n}_d = 1/\Omega \sum_{\mathbf{k}\neq 0} |\bar{v}_k|^2$.

### C. Self-consistent Bogoliubov approach for the quench dynamics

The quench of the soft-core interaction consists of two steps. The system is initially in the ground state of a weakly interacting BEC, i.e., $U_0 = 0$ when $t \leqslant 0$. At time $t > 0$ the Rydberg dressing is switched on immediately. The scheme is depicted in Fig. 1(c). The time dependence of the atomic interaction is described by a piecewise function as follows:

$$g_k = \begin{cases} g_0 & \text{when} \quad t \leqslant 0, \\ g_0 + U_0 f(k) & \text{when} \quad t > 0. \end{cases} \tag{6}$$

We assume that the $s$-wave interaction is not affected during the quench. Hence we use the parameter $\alpha = U_0/g_0$ to characterize the strength of the soft-core interaction with respect to the $s$-wave interaction.

A time-dependent Bogoliubov approach is applied to study the dynamics induced by the interaction quench. It is an extension of the conventional Bogoliubov approximation, where the canonical transformation becomes time dependent, $\hat{a}_{\mathbf{k}\neq 0}(t) = u_k(t)\hat{b}_{\mathbf{k}} - v_k(t)^* \hat{b}^\dagger_{-\mathbf{k}}$, where $u_k(t)$ and $v_k(t)$ are time-dependent amplitudes with the relation $|u_k(t)|^2 - |v_k(t)|^2 = 1$, which preserves the bosonic commutation relation. This approach has been widely used to study excitation dynamics in BECs with or without long-range interactions [10–12,14,20]. It provides a good approximation when the condensate has not undergone significant depletion.

Using the Heisenberg equation of the bosonic operators, we obtain the equations of motion of $u_k(t)$ and $v_k(t)$,

$$i\begin{bmatrix}\dot{u}_k(t) \\ \dot{v}_k(t)\end{bmatrix} = \begin{bmatrix}\epsilon_k + g_k n_c(t) & g_k n_c(t) \\ -g_k n_c(t) & -\epsilon_k - g_k n_c(t)\end{bmatrix}\begin{bmatrix}u_k(t) \\ v_k(t)\end{bmatrix}, \tag{7}$$

where $n_c(t)$ is the condensate density. The total density consists of the condensate and depletion densities as $n = n_c(t) + n_d(t)$, with the total density of the excitation, i.e., quantum depletion, given as

$$n_d(t) = \frac{1}{\Omega}\sum_k n_k(t) = \frac{1}{2\pi^2}\int_0^\infty n_k(t) k^2\, dk, \tag{8}$$

where $n_k(t) \equiv \langle \hat{a}^\dagger_{\mathbf{k}} \hat{a}_{\mathbf{k}}\rangle = |v_k(t)|^2$ is the distribution of momentum states. When the excitation from the condensate is weak, $n_d \approx 0$, we can approximate $n_c(t) \approx n$. Equation (7) can be solved exactly,

$$\begin{bmatrix}u_k(t) \\ v_k(t)\end{bmatrix} = \left[\cos(E_k(t)t)\mathbb{I} - i\frac{\sin(E_k(t)t)}{E_k(t)} \times \begin{pmatrix}\epsilon_k + g_k n_c(t) & g_k n_c(t) \\ -g_k n_c(t) & -\epsilon_k - g_k n_c(t)\end{pmatrix}\right]\begin{bmatrix}u_k(0) \\ v_k(0)\end{bmatrix}, \tag{9}$$

where $\mathbb{I}$ is the identity matrix, and the dispersion relation $E_k(t) = \sqrt{\epsilon_k[\epsilon_k + 2g_k n_c(t)]}$. The initial values of $u_k(t)$ and $v_k(t)$ are [3]

$$u_k(0) = \sqrt{\frac{1}{2}\left[\frac{\epsilon_k + g_0 n}{E_k(0)} + 1\right]},$$
$$v_k(0) = -\sqrt{\frac{1}{2}\left[\frac{\epsilon_k + g_0 n}{E_k(0)} - 1\right]}. \tag{10}$$

We kept $n_c(t)$ explicitly in Eq. (9) to indicate that $u_k(t)$ and $v_k(t)$ are time-dependent quantities, while the total density $n$ is time independent. Using the time-dependent solutions, we calculate the momentum distribution $n_k(t)$,

$$n_k(t) = |v_k(0)|^2 + g_k n_c(t)[g_k n_c(t) - g_0 n] \times \frac{\epsilon_k[1 - \cos(2E_k(t)t)]}{2E_k(t)^2 E_k(0)}. \tag{11}$$

Equation (11) shows that $n_k(t)$ encodes the dispersion relation. One can see this after carrying out a Fourier transform of $n_k(t)$ to the frequency domain [50].

As we consider very weak quantum depletion, the conventional Bogoliubov approach can already describe the dynamics well. To take into account the corrections due to the weak quantum depletion, we additionally employ a self-consistent method through iterative calculations. From Eq. (9), we obtain the quantum depletion and hence $n_c(t)$. As we still have $n_c(t) \approx n$, $n_c(t)$ will be treated as an adiabatically changing quantity such that we can again use Eq. (9) to calculate the quantum depletion in which the weak time dependence of $n_c(t)$ is considered. This procedure is iterated until $n_c(t)$ is self-consistently obtained, i.e., additional iterations will no longer change $n_c(t)$. Note that the procedure used here is approximately applicable, as the quantum depletion is small. When the depletion is strong, one could apply the rigorous self-consistent procedure presented in Ref. [12].

In the following calculations, we scale the energies, lengths, and times with respect to the interaction energy $g_0 n$, coherence length $\zeta = (m g_0 n)^{-1/2}$, and coherence time $\tau = t g_0 n$ of the initial condensate. The zero-range interaction strength is fixed by the $s$-wave scattering length. To be concrete we set $a_s = 0.1 n^{-1/3}$ throughout this work.

## III. RESULTS AND DISCUSSION

### A. Stationary dispersion relation

The soft-core interaction drastically alters the dispersion relation of the Bogoliubov excitations. To illustrate this, we first examine dispersion relations of a static BEC by assuming that the soft-core interaction is present. When the soft-core

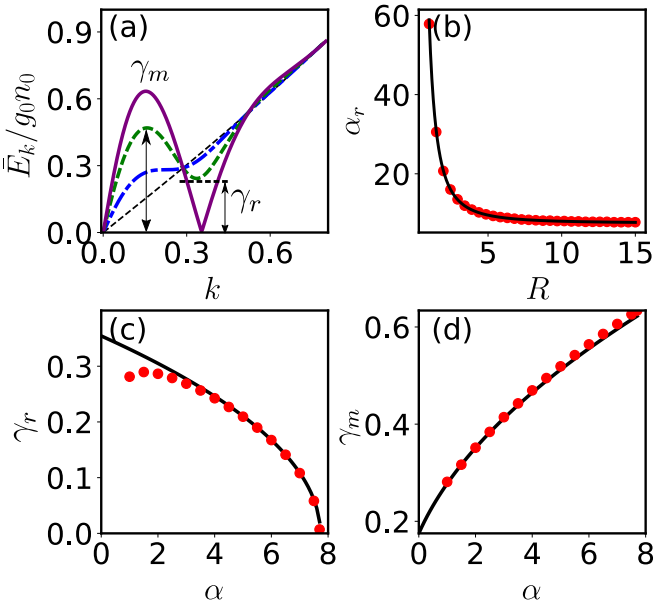


FIG. 2. Roton and maxon modes. (a) Bogoliubov spectra in the stationary state for $\alpha = 0$ (thin dashed black line), $\alpha = 1$ (dot-dashed blue line), $\alpha = 6$ (thick dashed green line), and $\alpha = 7.7$ (solid purple line), when $R = 15$. The energy gaps $\gamma_r$ and $\gamma_m$, indicating, respectively, the roton and maxon energies are marked for the green curve. For $\alpha > 7.7$, the spectra become unstable. (b) Critical value $\alpha_r$ vs $R$. Analytical calculations (black line) agree with the numerical data (dotted red line). (c) Roton energy $\gamma_r$. With an increase in $\alpha$, the roton energy decreases. For large $\alpha$, the analytical (solid black line) and numerical (dotted red line) results agree. At small $\alpha$, roton minima become weak and eventually disappear, which leads to the deviation. Data points in red are the energies taken numerically from the dispersion. (d) The maxon energy $\gamma_m$ increases with $\alpha$. The analytical (solid black line) and numerical data agree nicely. In (c) and (d) $R = 15$.

interaction is weak, i.e., $\alpha$ is small, the dispersion relation resembles that of a weakly interacting BEC. The excitation energies increase monotonically with momentum $k$ [3] [see Fig. 2(a)]. Upon increasing $\alpha$, the shape of the Bogoliubov spectra changes significantly. For different $\alpha$ values, the dispersion intersects at a momentum determined by $V(k) = 0$ [see Fig. 1(b)], where the mode energies of the Rydberg-dressed BEC coincide with that of a weakly interacting BEC (dashed curve). More importantly, a local maximum and minimum can be seen in the dispersion relation when $\alpha$ is large [Fig. 2(a)]. At the maximum, special modes called maxon modes form, while roton modes emerge around the minima [23]. In the following, we denote the energies of the maxons and rotons $\gamma_m$ and $\gamma_r$, as the local maximal and minimal values of the dispersion relation.

The roton and maxon modes depend on the soft-core interaction nontrivially. With increasing $\alpha$, $\gamma_r$ decreases while $\gamma_m$ increases, as shown by the examples in Fig. 2(a). For sufficiently large $\alpha$, the roton gap vanishes as the energies become complex. Due to the roton instability, the homogeneous state becomes dynamically unstable, which leads to interesting physics. It has been shown that the emergence of the roton instability can cause a first-order phase transition where the ground state changes from a uniform condensate to a supersolid state [35,51,52]. We note that instabilities in dipolar BECs are caused by angular-dependent interactions with both attractive and repulsive components [16], while the instability in the dressed BEC is induced by stronger, isotropic interactions. We show in the following section that switching on the dressed interaction induces exotic dynamics even without triggering the roton instability.

We now obtain the critical value at which the roton mode becomes unstable. In Fig. 1(b), the Fourier transform of the soft-core potential has the most negative value around $k_r \approx 5\pi/3R$. The roton minimum takes place around this momentum. By substituting $k_r$ into the dispersion relation, we can identify the critical $\alpha$ at which the roton energy becomes complex:

$$\alpha_r = \frac{5e^{5\pi/3}(36R^2 + 25\pi^2)}{72\pi R^2\left[2e^{5\pi/6}\sin\left(\frac{\pi}{6} - \frac{5\pi}{2\sqrt{3}}\right) - 1\right]}. \tag{12}$$

To check the accuracy of this critical value, we numerically find the instability point from the dispersion relation for various $\alpha$ values. Both numerical and analytical values are shown in Fig. 2(b). The analytical result agrees with the numerical values very well. This supports the assumption that the roton minimum happens around momentum $k_r$.

Knowing the momentum $k_r$, we can obtain the roton energies by inserting it into Eq. (4). It is found that the roton energy $\gamma_r$ decreases with increasing $\alpha$ [see Fig. 2(c)]. The roton energy from the numerical calculations agrees with the analytical data, especially when the soft-core interaction is strong. Decreasing the soft-core interaction, the roton modes disappear for sufficiently small $\alpha$, as our numerical calculations indicate. Here large deviations between the two methods are found in this regime.

On the other hand, the location of the maxon modes in momentum space is difficult to find. By analyzing the dispersion relation, the momentum corresponding to the maxon mode is approximately given by $k_m \approx k_r/2$. Using this approximation, we substitute this momentum value into Eq. (4) and calculate the maxon energy. The result is shown in Fig. 2(d), where the approximate value matches the numerical values with a high degree of accuracy.

Recently, the stationary states of 2D and 3D Rydberg-dressed BECs have been examined [53]. It was shown that the increased occupation around the roton modes leads to instabilities in the ground state in the form of density waves. It was also shown that the strong interparticle interactions lead to a large depletion of the condensate.

### B. Roton and maxon excitation

Depending on the parameters of the soft-core interaction, the stationary dispersion relation could support roton and maxon modes. One example is displayed in Fig. 3(a). Now if we quench the interaction, the dispersion relations of the initial and final states are different. The system is driven out of equilibrium, such that the momentum distributions $n_k(\tau)$ evolve with time. In Fig. 3(b), snapshots of the momentum density $n_k(\tau)k^2$ are shown. At $\tau = 0$, the BEC is in a stationary state, which depends on the initial condition, $\bar{v}_k$. The respective momentum density is a smooth function of

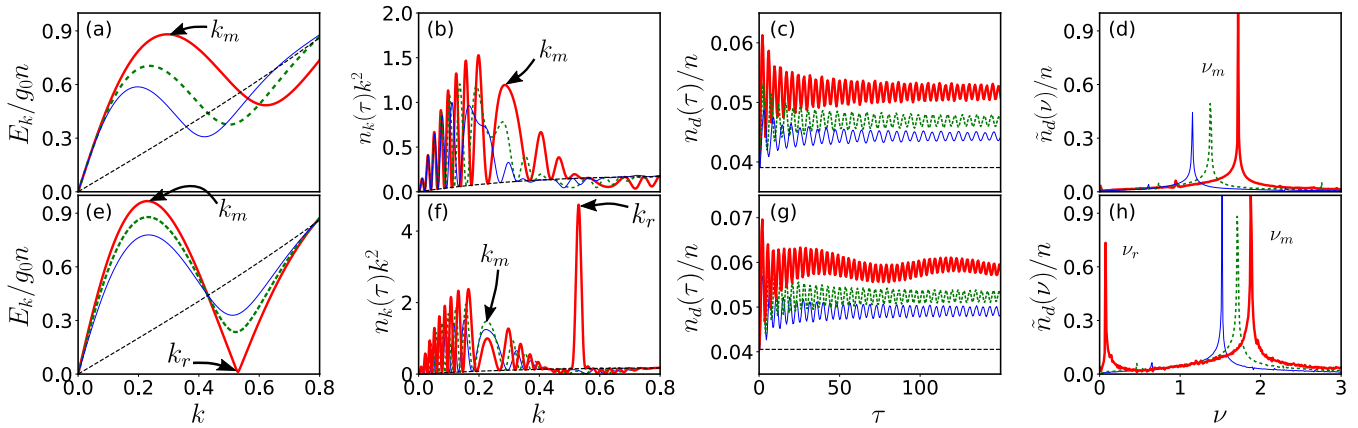


FIG. 3. Excitation of the roton and maxon modes. (a) Dispersion for a static BEC. The momentum of the roton and maxon modes decreases with increasing soft-core radius $R$. Without soft-core interactions, the excitation energy monotonically increases with the momentum (thin dashed black curve). The location of the maxon modes for the red curve is highlighted by the arrow. (b, c) The interaction quench is applied. Momentum densities $n_k k^2$ at time $\tau = 30$ are shown in (b). The dashed black curve shows the momentum distribution of the initial state. The quantum depletion damps slightly at early times and then oscillates rapidly with negligible damping over a long time (c). (d) This leads to sharp peaks in the respective Fourier transformation. The nonzero width of the peaks results from the damping at the early stage of the evolution. The frequency $\nu_m$ at the major peaks is determined by the maxon frequency. Minor peaks corresponding to other frequencies are almost invisible. In (a)–(d), three soft-core radii, $R = 8$ (thick solid red curve), $R = 10$ (thick dashed green curve), and $R = 12$ (thin solid blue curve), are considered, while the interaction strength is fixed at $\alpha = 4$. (e) Dispersion, (f) momentum distribution, (g) quantum depletion, and (h) Fourier transformation of the quantum depletion for $R = 10$ and $\alpha = 5$ (thin solid blue curve), $\alpha = 6.5$ (thick dashed green curve), and $\alpha = 7.99$ (thick solid red curve). Approaching the roton instability (e), the momentum density distribution (f) develops a large occupation around modes at $k_r$ at $\tau = 30$. Both the roton and the maxon momenta are highlighted by arrows in this case. The depletion dynamics maintains a slower oscillation (g) as the interaction strength is increased, which can be seen from the Fourier transformation of the quantum depletion (h). The lower peak frequency $\nu_r$ is determined by the roton mode. The major peaks at higher frequencies are due to the excitation of maxons. When $\alpha = 7.99$, both the roton and the maxon modes are dynamically stable, giving narrow Fourier spectra. While the above spectra were calculated, the system was allowed to evolve up to time $\tau = 600$.

$k$. When $t > 0$, different momentum states are modified by the presence of the soft-core interaction, causing dynamical evolution of the quantum depletion.

The dynamics of the quantum depletion depends vitally on the parameters $R$ and $\alpha$ in the soft-core interaction. After switching on the interaction, the excitation of the Bogoliubov modes significantly affects the momentum distribution. We first investigate the oscillatory behavior of the quantum depletion. For moderate soft-core interactions, many momentum modes are excited by the soft-core interaction, as shown in Fig. 3(b). The quantum depletion increases rapidly at short times and then oscillates around a constant value [Fig. 3(c)]. Its amplitude decreases slowly when $\tau < 100$ but then reaches a constant. The Fourier transformation $\tilde{n}_d(\nu)$ of the quantum depletion, characterizing the spectra of the dynamics, shows a sharp peak [Fig. 3(d)]. The finite width of the peak is largely due to the damping of the quantum depletion at the early stage of the evolution. The peak positions, i.e., frequency of the oscillations, decrease gradually when the soft-core radius is increased.

For stronger soft-core interactions, the roton mode moves towards the instability point [see Fig. 3(e)]. As the interaction strength approaches $\alpha_r$, the momentum density develops a large occupation at momentum values matching $k_r$ [see Fig. 3(f)]. Around the maxon momentum $k_m$, there are also large occupations. A new, lower-frequency pattern develops on top of the fast oscillation in the quantum depletion [Fig. 3(g)]. This changes the Fourier spectra of the quantum depletion, where a new peak is found at a lower frequency [Fig. 3(h)].

Importantly, the peak positions in $\tilde{n}_d(\nu)$ are determined by the roton and maxon energies, where fast oscillations are due to the excitations of the maxon modes, while slow oscillations are due to the roton modes. To verify this, we first obtain the maxon and roton frequencies by substituting the corresponding momenta $k_m$ and $k_r$ into Eq. (4). We then compare them with the frequency at the peak positions in the Fourier spectra. Note that the oscillation frequency (i.e., peak frequency of the Fourier spectra) in the quantum depletion is twice the Bogoliubov energy, as can be seen in Eq. (11). As shown in Fig. 4, the numerical data for both the maxon mode [Figs. 4(a) and 4(b)] and the roton mode [Figs. 4(c) and 4(d)] agree with the analytical calculations. When the interaction strength is varied, the maxon (roton) frequency increases (decreases) with increasing $\alpha$. If we increase the soft-core radius, the frequencies of both modes decrease.

The agreement between numerical and analytical calculations confirms that both roton and maxon modes are excited via quenching of the soft-core interaction. The dynamically excited modes are stable, as both the fast and the slow oscillations are *persistent* for a long time. In our numerical simulations, the oscillations will not dampen even when the simulation time $\tau > 1000$. Such persistent oscillatory dynamics also leads to the sharp peaks in the Fourier transformation of the quantum depletion.

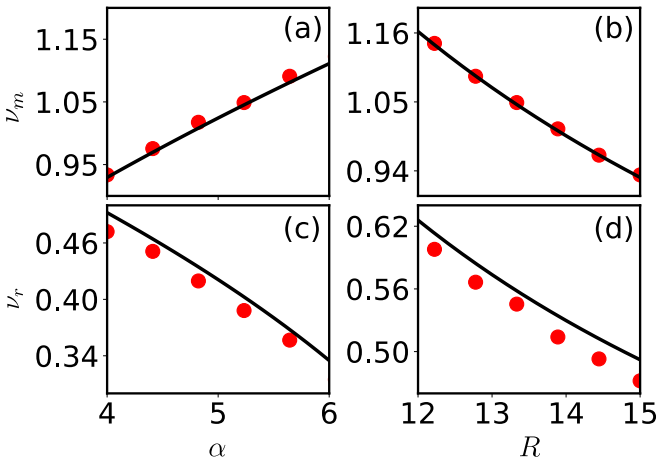


FIG. 4. (a, b) Maxon frequency and (c, d) roton frequency. Circles represent numerical data from the Fourier spectra. Solid curves are the analytical results $2\gamma_m$ in (a) and (b) and $2\gamma_r$ in (c) and (d) obtained from the Bogoliubov dispersion. The maxon (roton) frequency increases (decreases) with increasing interaction strength. At the critical point $\alpha_r$, the roton mode loses stability. The frequencies of both modes tend towards 0 for larger $R$ values as the soft-core interaction becomes weaker. In (a) and (c) $R = 15$. In (b) and (d) $\alpha = 4$.

We want to emphasize that the quench dynamics in the dressed BEC is in sharp contrast to BECs with either $s$-wave or dipolar interactions. In a weakly interacting BEC, the quantum depletion grows exponentially to a steady value $\propto \zeta^{-\frac{1}{3}}$, while oscillatory patterns are not present in the depletion [11], due to the fact that low-energy phonon modes dominate the quench dynamics. In dipolar BECs [19,20,24,54,55], on the other hand, roton modes are formed due to the interplay between long-range dipolar and $s$-wave interactions [19,20,24,54,55]. These roton modes can be excited by quenching of the dipolar interaction, while maxon modes are typically unstable in the dynamics (see Appendix A for examples).

### C. Quantum depletion in the long-time limit

In the long-time limit $\tau \gg 1$, the quantum depletion oscillates rapidly around a mean value [Figs. 3(c) and 3(g)]. In the following, we evaluate the asymptotic value of the quantum depletion. First, we derive an analytic expression using the following approximations. In the long-time limit, the time-averaged quantum depletion is largely determined by the low-momentum modes. Moreover, we neglect the oscillation terms in Eq. (11), as they are related to the rotons and maxons. Using these approximations, the asymptotic form of the momentum distribution $n_k^\infty$ is obtained,

$$n_k^\infty \approx \frac{1}{2}\left(\frac{k^2+1}{\sqrt{k^2(k^2+4)}} - 1\right) + \frac{\alpha f(k)}{4k}\frac{n_c s^\infty}{n}, \tag{13}$$

where $n_c s^\infty$ is the asymptotic condensate density. After carrying out the integral over momentum space, the approximate

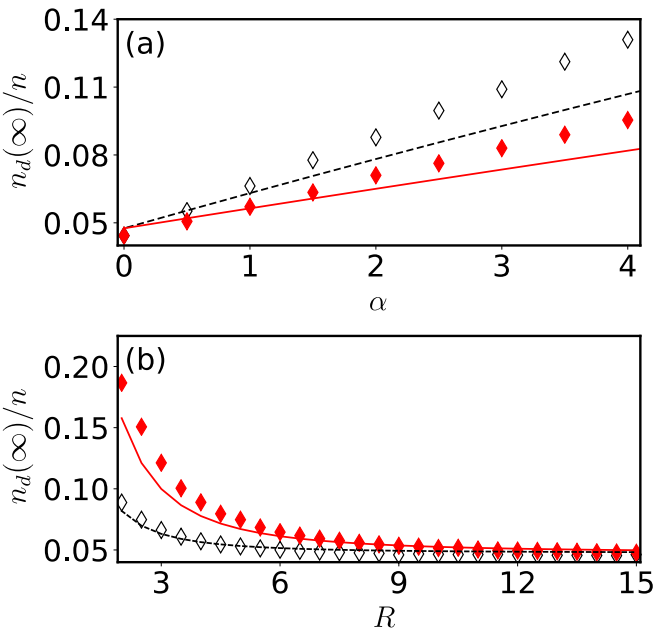


FIG. 5. Asymptotic quantum depletion. (a) The asymptotic quantum depletion increases with increasing $\alpha$, which is shown by both the analytical and the numerical calculations. (b) The quantum depletion $n_d^\infty$ decreases with increasing soft-core radius. The lines are found analytically using Eq. (14), while the data points are found by numerically solving Eq. (8) and taking the mean value at later times between $\tau \approx 50$ and $\tau \approx 150$. Parameters in (a) are $R = 3$ (open black diamonds, dashed line) and $R = 4$ (filled diamonds, solid line). Parameters in (b) are $\alpha = 1$ (open black diamonds, dashed line) and $\alpha = 3.5$ (filled red diamonds, solid line).

quantum depletion when $\tau \to \infty$ is obtained,

$$\frac{n_d^\infty}{n} \approx 2\Gamma\left(\frac{R^2+\alpha\pi}{3R^2+2\pi\alpha\Gamma}\right), \tag{14}$$

where $\Gamma = (2\pi^2\zeta^3 n)^{-1}$. This result predicts that the quantum depletion approaches a constant value $n_d^\infty/n \to 2\Gamma/3$ in the limit $R \to \infty$. This resembles the result of the weakly interacting BEC, i.e., the soft-core interaction plays no role in the dynamics.

To verify the analytical calculation, we numerically find the mean value of the quantum depletion when the time is large. Both the numerical and the analytical results are shown in Fig. 5. For small $\alpha$, low-momentum states are populated by switching on the soft-core interaction. This is the regime where the approximation works. Here we find a good agreement between the numerical and the analytical calculations. With an increasing interaction strength, more and more higher-momentum components are populated [see Fig. 3(f)], causing larger depletion. When $\alpha$ is fixed, the quantum depletion decreases with increasing $R$, as shown in Fig. 5(b). This results from the fact that the quench only affects momentum components $k < k_r/R$ [see Fig. 1(b)]. For momentum $k \gg k_r/R$, the dispersion is largely unaffected by the soft-core interaction as the respective $V(k) \to 0$. Therefore increasing $R$ leads to a weaker quantum depletion.

## IV. CONCLUSION

We have studied the dynamics of 3D BECs in free space, with Rydberg-dressed soft-core interactions. An interaction quench is implemented by turning on the soft-core interaction instantaneously, starting from a weakly interacting BEC. The Bogoliubov spectrum of the BEC displays local maxima and minima, which are identified as maxon and roton modes. Through a time-dependent Bogoliubov approach, we have calculated the dynamics of the quantum depletion self-consistently. Our results show that both roton and maxon modes are excited by switching-on of the soft-core interaction. The excitation of roton and maxon modes generates slow and fast oscillatory dynamics in the quantum depletion. Our simulations show that the excited roton and maxon modes are stable in the presence of the soft-core interaction, which is observed from the persistent oscillations of the quantum depletion. We have found the frequencies of the roton and maxon modes approximately, and they are confirmed by the numerical simulations.

Our study shows that exotic roton and maxon excitations can be created in Rydberg-dressed BECs through interaction quenches. Properties of the maxons and rotons can also be seen from condensate fluctuations (see Appendix B for details) and density-density correlations (see Appendix C). The results studied in this work might be useful in identifying the soft-core interaction, by measuring the frequencies and strength of the quantum depletion. In the future, it would be worth studying the stability of the maxon mode due to Beliav damping [56,57]. Maxon modes are also present in strongly correlated $^4$He [58,59], where the maxon decays into phonons at the Pitaevskii plateau. Whether the maxons in Rydberg-dressed BECs will decay through this mechanism is an open and interesting research question. Another interesting question is whether the soft-core interaction can lead to the formation of droplets in Rydberg-dressed BECs.

## ACKNOWLEDGMENTS

We thank Yijia Zhou and S Kumar Mallavarapu for fruitful discussions. The research leading to these results received funding from EPSRC Grant No. EP/R04340X/1 via the QuantERA project "ERyQSenS," UKIERI-UGC Thematic Partnership No. IND/CONT/G/16-17/73, and the Royal Society through International Exchanges Cost Share Award No. IEC\NSFC\181078. We are grateful for access to the Augusta High Performance Computing Facility at the University of Nottingham.

## APPENDIX A: DYNAMICS OF 2D DIPOLAR SYSTEMS

Quench dynamics in BECs with dipolar interactions are drastically different. The dipolar interaction is given by

$$\tilde{V}_{\rm dd}(\mathbf{r}-\mathbf{r}') = g_0\delta(\mathbf{r}) + \frac{d^2}{|\mathbf{r}-\mathbf{r}'|^3}[1-3\cos^2(\theta)], \quad \text{(A1)}$$

where $d$ is the dipole moment, $\theta$ is the angle between the dipoles and the molecular axis, and $g_0$ is the short-range contact interaction as before. In three dimensions, the Fourier transform of the dipolar interaction has no momentum dependence [19]. In a 2D trapped dipolar Bose gas [17,18], the interaction potential displays a strong momentum dependence [20].

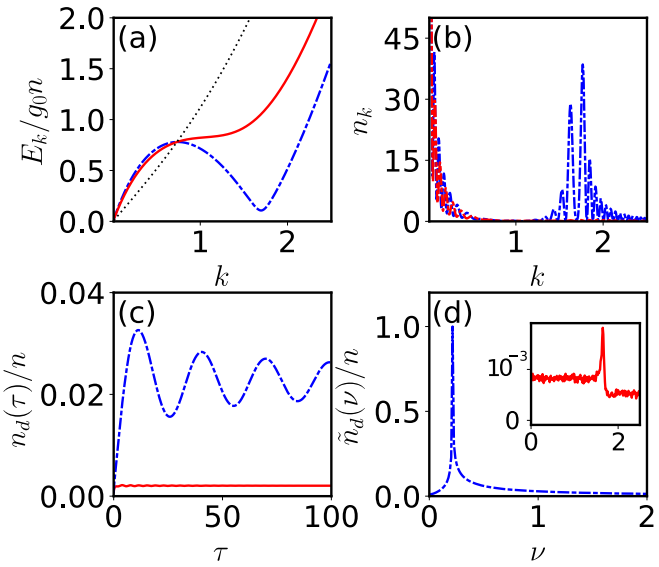


FIG. 6. Quantum depletion in a dipolar BEC. Solid red curves represent $\alpha_d = 2.1$; dashed blue curves, $\alpha_d = 2.7$. Black dashes correspond to the noninteracting dispersion relation. The axial confinement is set to $l_z = 0.1n^{-1/2}$. We show the dispersion relation in (a), while the momentum distribution at time $\tau = 30$ is shown in (b). The quantum depletion and corresponding Fourier spectra are shown in (c) and (d), respectively. Inset: A maxon mode is excited for $\alpha_d = 2.1$. However, the signal is very weak and almost invisible. The axes in the inset are the same as in (d).

We consider a quasi-2D setup [20], where a strong confinement is applied in the perpendicular $z$ direction while atoms are left free to move in the $x$-$y$ plane. The dipoles are polarized along this $z$ axis. This leads the axial confinement as $l_z$, which provides a natural rescaling of $\mathbf{r} \mapsto \mathbf{r}/l_z$ [17,18,20–22]. After integrating Eq. (A1) in the $z$ axis, we obtain the Fourier transformation of the quasi-2D dipolar interaction [20]

$$g_{\rm dd}(k) = g_0 + d^2[2 - 3k\sqrt{\pi}\,{\rm Erfc}(k)e^{k^2}], \quad \text{(A2)}$$

where ${\rm Erfc}(k)$ is the complementary error function. A dimensionless parameter $\alpha_d = 2\pi d^2/3g_0$ is used to characterize the strength of the dipolar interactions, such that the interaction after the quench is given as $g_{\rm dd}(k)/g_0 = 1 + \alpha_d[2 - 3k\sqrt{\pi}\,{\rm Erfc}(k)e^{k^2}]$. The quench scheme for the dipolar case is similar to the procedure outlined in the text. We switch on the dipolar interaction instantaneously, while keeping the $s$-wave interaction unchanged.

The dispersion relation for the dipolar BEC is shown in Fig. 6(a), where both roton and maxon modes are shown.

When the dipolar interaction is compared to the Rydberg-dressed BEC [e.g., Fig. 2(a)], the energies of the low-momentum modes remain low, as shown by directly comparing the dispersion relations. The absence of these high maxon energies means that the mechanism behind the dipolar interactions prevent the oscillations that we previously attributed to the maxon modes from reaching high amplitudes [Fig. 6(b)] [20,21,60].

The energy spectrum of dipolar BECs [Fig. 6(a)] shows that the maxon energies are slightly above the energy of a weakly interacting BEC (dashed black line). In comparison, Fig. 2(a) in the text shows that the maxon energy in the Rydberg-dressed interaction is much higher. The absence of high-frequency oscillations in the dipolar BECs might be attributed to this lack of high-energy maxon modes.

We follow the same self-consistent process to obtain the condensate fraction. We calculate the quantum depletion as before, as $n_d/n = 1/(2\pi l_z^2 n)\int_0^\infty n_k k\, dk$. When $\alpha_d$ is small, the dynamics develops maxon oscillations, which dampens in short time scales, as shown in Fig. 6(c). When $\alpha_d$ is large, the roton frequency completely overpowers the maxon frequency in the dynamics. The absence of a stable maxon mode is also seen in the Fourier spectra [Fig. 6(d)].

## APPENDIX B: CONDENSATE FLUCTUATION

In this section, we evaluate the fluctuation of the condensate for the Rydberg-dressed BEC. The condensate fluctuation is defined as

$$\begin{aligned}\Delta n_c &= \sqrt{\langle n_c^2\rangle - \langle n_c\rangle^2}\\ &= \sqrt{\langle n_d^2\rangle - \langle n_d\rangle^2}\\ &= \frac{1}{\Omega}\sqrt{\sum_{\mathbf{k}\mathbf{k}'\neq 0}\left[\langle \hat{a}^\dagger_{\mathbf{k}}\hat{a}_{\mathbf{k}}\hat{a}^\dagger_{\mathbf{k}'}\hat{a}_{\mathbf{k}'}\rangle - \langle \hat{a}^\dagger_{\mathbf{k}}\hat{a}_{\mathbf{k}}\rangle\langle \hat{a}^\dagger_{\mathbf{k}'}\hat{a}_{\mathbf{k}'}\rangle\right]},\end{aligned}$$

where we have assumed that the total density $n$ is a constant. Using the Bogoliubov transformation, the fluctuation of the condensate is obtained:

$$\Delta n_c = \frac{1}{\Omega}\sqrt{2\sum_{\mathbf{k}\neq 0} n_k(1+n_k)}. \tag{B1}$$

One can numerically evaluate the fluctuation by inserting Eq. (11) into the above equation. For convenience, the relative fluctuation, $\sqrt{N}\Delta n_c/n$, is calculated. Some examples are shown in Fig. 7(a). The fluctuation increases rapidly and then saturates at an asymptotic value when the time is large. The fluctuation oscillates around the asymptotic value. The maxon modes lead to fast oscillations. When the roton mode is significantly populated, a slower oscillation is found.

The asymptotic value of the fluctuation depends on the soft-core interaction. With increasing $\alpha$, the asymptotic value increases [see Figs. 7(a) and 7(b)]. We can estimate the asymptotic value of the density fluctuation by replacing $n_k$ with its asymptotic value, Eq. (13), in Eq. (B1), which yields

$$\frac{\sqrt{N}\Delta n_c s^\infty}{n} = \sqrt{2\Gamma\int_0^\infty n_k^\infty\left[1+n_k^\infty\right]k^2 dk}. \tag{B2}$$

Further assuming that the fluctuation depends solely on low-momentum states, we obtain the approximate result of the fluctuation when $\tau\to\infty$,

$$\frac{\sqrt{N}\Delta n_c s^\infty}{n} \approx \sqrt{\frac{2\Gamma\pi^2[1+\pi^2\alpha(6\sqrt{3}+\pi\alpha C)]}{27R}}, \tag{B3}$$

with the constant $C = [4\sqrt{3}\pi - 3\log(\frac{27}{16})]$. The approximation result shows that fluctuation of the condensate decreases (increases) with increasing $R$ ($\alpha$). In Figs. 7(b) and 7(c), numerical and approximate results are both shown. The two calculations agree when $\alpha$ is small or $R$ is large, where the depletion and fluctuation are both small. Though a large discrepancy is found when $\alpha$ is large or $R$ is small, the trends found from both numerical and analytical calculations are the same.

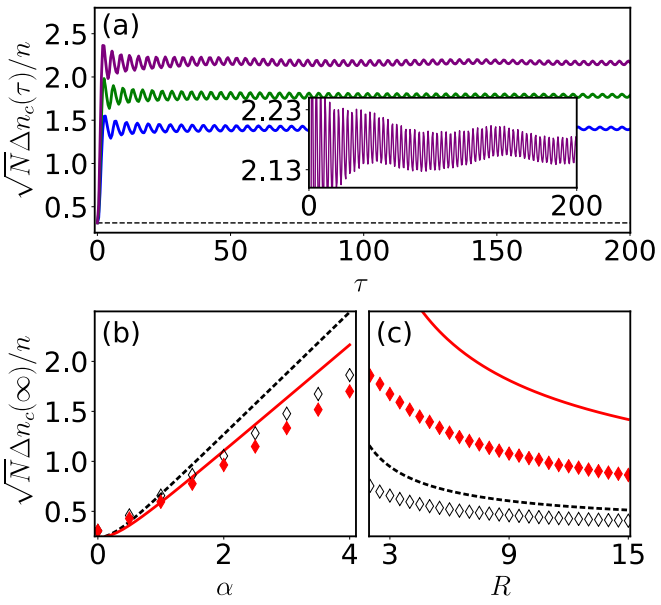


FIG. 7. Condensate fluctuation. (a) Dynamics of the condensate fluctuation. We fix $R = 10$ and evolve the system for $\alpha = 5$ (lower, blue curve), $\alpha = 6.5$ (middle, green curve), and $\alpha = 7.99$ (upper, purple curve). The dashed line is the fluctuation without the soft-core interaction, i.e., $\alpha = 0$. Inset: Fluctuations when $\alpha = 7.99$, highlighting the low-frequency oscillations due to rotons. The axes in the inset are the same as in (a). Mean values of the fluctuations for different (b) $\alpha$ and (c) $R$ when the time $\tau\to\infty$. We consider $R = 3$ (open black diamonds, dashed line) and $R = 4$ (filled red diamonds, solid line) in (b) and $\alpha = 1$ (open black diamonds, dashed line) and $\alpha = 3.5$ (filled red diamonds, solid line) in (c). Diamonds correspond to the numerical data, while lines represent the analytical expression. Other parameters can be found in Fig. 5 in the text.

## APPENDIX C: DENSITY-DENSITY CORRELATION

Finally, we evaluate the density-density correlation function [10,11]

$$g^{(2)}(\mathbf{r},t) = \sum_{\mathbf{k},\mathbf{k}',\mathbf{q}} e^{i\mathbf{k}.\mathbf{r}}\frac{1}{\Omega^2}\langle \hat{a}^\dagger_{\mathbf{k}+\mathbf{q}}(t)\hat{a}_{\mathbf{k}}(t)\hat{a}^\dagger_{\mathbf{k}'-\mathbf{q}}(t)\hat{a}_{\mathbf{k}'}(t)\rangle. \tag{C1}$$

Within the Bogoliubov transformation, this can then be expressed in terms of the condensate density as $\langle 1/\Omega^2\sum_{\mathbf{k},\mathbf{k}'}\hat{a}^\dagger_{\mathbf{k}+\mathbf{q}}(t)\hat{a}_{\mathbf{k}}(t)\hat{a}^\dagger_{\mathbf{k}'-\mathbf{q}}(t)\hat{a}_{\mathbf{k}'}(t)\rangle = n^2 + n/\Omega\sum_{\mathbf{k}}[4|v_{\mathbf{k}}|^2 - u^*_{\mathbf{k}}v_{\mathbf{k}} - u_{\mathbf{k}}v^*_{\mathbf{k}}]$. Defining $D = |\mathbf{r}-\mathbf{r}'|/\zeta$ as the scaled interatomic distance, the correlation function is given as [11]

$$g^{(2)}(D,\tau) - 1 = \frac{4\Gamma}{D}\int_0^\infty k\, dk\sin(kD) \times\left[n_k - \mathrm{Re}[u^*_k(\tau)v_k(\tau)]\right]. \tag{C2}$$

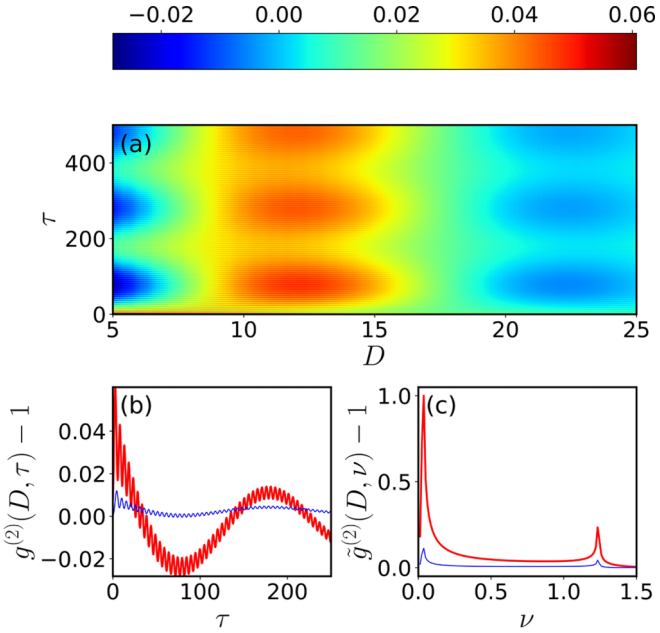


FIG. 8. Density-density correlation. (a) Density-density correlations as a function of $D$ and $\tau$, with $R = 15$ and $\alpha = 7.7$. (b) Correlations at $D = 5$ (thick red curve) and $D = 25$ (thin blue curve) (c) Corresponding Fourier spectrum of the correlation function. In the Fourier spectra, the peaks at lower and higher frequencies are due to the excitation of roton and maxon modes.

We see in Fig. 8(a) that the correlations immediately develop both slow and fast oscillations. The slow oscillations correspond to the excitation of roton modes when $\gamma_r$ is small. The fast oscillations attributed to the maxon occupation are more easily observed when looking at a specific value of $D$ [Fig. 8(b)]. The corresponding Fourier transformation $\tilde{g}^{(2)}(D, \nu) - 1$ clearly shows the associated frequency peaks. When the distance $D < R$, $g^{(2)}(D, \tau) - 1$ oscillates with high amplitudes and can have negative values, i.e., strong repulsive interactions lead to anticorrelations. Around the soft-core radius, the correlations are positive and reach their maximal values. When $D \gg R$, the correlations tend to 0 at large times.

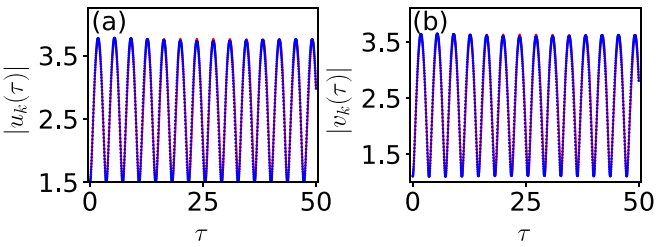


FIG. 9. Evolution of Bogoliubov amplitudes. Using the same parameters as the thick red curve in Fig. 3(g), the amplitudes (a) $|u_k(\tau)|$ and (b) $|v_k(\tau)|$ are shown for $k = 0.3$. Solid red curves correspond to our self-consistent algorithm, while blue dots are obtained by the rigorous calculation from Ref. [12].

## APPENDIX D: SELF-CONSISTENT CALCULATION COMPARISON

The dynamical condensate density is found by calculating the quantum depletion self-consistently. In our calculation we have chosen parameters such that quantum depletion is small in the initial state and also in the dynamical evolution. With this condition at hand, the calculation is carried out by treating $n_c$ as an adiabatically changing parameter. Here a crucial step in the derivation of Eq. (9) in the text is that we assume $n_c = n$ during the first iteration. With this crude approximation, Eq. (7) can be integrated, leading to Eq. (9). After the first iteration, the value of $n_c$ is updated and then reinserted into the next iteration in Eq. (9). As the corrected $n_c$ is still very close to $n$, we directly iterate Eq. (9) instead of solving Eq. (7) numerically.

A more rigorous approach was presented in Ref. [12] and should be followed in the event of large quantum depletion. Due to $n_c \approx n$, we can replace the phase term

$$\phi = \int_0^t dt' n_c(t') \tag{D1}$$

in Ref. [12] with $n_c t$ in our calculations. These two calculations appear to agree well when using the parameter regimes considered in the work. Some examples are given in Fig. 9, where we show the dynamical evolution of $u_k(t)$ and $v_k(t)$ obtained by the two different calculations. The blue curves are obtained from the rigorous approach used in Ref. [12], and the red curves using our calculations.

[1] E. L. Bolda, E. Tiesinga, and P. S. Julienne, Phys. Rev. A **66**, 013403 (2002).
[2] D. Jaksch and P. Zoller, Ann. Phys. (NY) **315**, 52 (2005).
[3] C. J. Pethick and H. Smith, *Bose-Einstein Condensation in Dilute Gases* (Cambridge University Press, Cambridge, UK, 2008).
[4] L. Pitaevskii and S. Stringari, *Bose-Einstein Condensation and Superfluidity* (Oxford University Press, New York, 2016).
[5] T. D. Lee, K. Huang, and C. N. Yang, Phys. Rev. **106**, 1135 (1957).
[6] R. Lopes, C. Eigen, N. Navon, D. Clément, R. P. Smith, and Z. Hadzibabic, Phys. Rev. Lett. **119**, 190404 (2017).
[7] J. Stenger, S. Inouye, M. R. Andrews, H. J. Miesner, D. M. Stamper-Kurn, and W. Ketterle, Phys. Rev. Lett. **82**, 2422 (1999).
[8] W. Ketterle, S. Inouye, M. R. Andrews, J. Stenger, H.-J. Miesner, and D. M. Stamper-Kurn, Nature **392**, 151 (1998).
[9] P. Makotyn, C. E. Klauss, D. L. Goldberger, E. A. Cornell, and D. S. Jin, Nat. Phys. **10**, 116 (2014).
[10] G. I. Martone, P. É. Larré, A. Fabbri, and N. Pavloff, Phys. Rev. A **98**, 063617 (2018).
[11] S. S. Natu and E. J. Mueller, Phys. Rev. A **87**, 053607 (2013).
[12] X. Yin and L. Radzihovsky, Phys. Rev. A **88**, 063611 (2013).

[13] A. G. Sykes, J. P. Corson, J. P. D'Incao, A. P. Koller, C. H. Greene, A. M. Rey, K. R. A. Hazzard, and J. L. Bohn, Phys. Rev. A **89**, 021601(R) (2014).
[14] B. Kain and H. Y. Ling, Phys. Rev. A **90**, 063626 (2014).
[15] C. R. Cabrera, L. Tanzi, J. Sanz, B. Naylor, P. Thomas, P. Cheiney, and L. Tarruell, Science **359**, 301 (2018).
[16] L. Santos, G. V. Shlyapnikov, P. Zoller, and M. Lewenstein, Phys. Rev. Lett. **85**, 1791 (2000).
[17] U. R. Fischer, Phys. Rev. A **73**, 031602(R) (2006).
[18] C. Ticknor, R. M. Wilson, and J. L. Bohn, Phys. Rev. Lett. **106**, 065301 (2011).
[19] T. Lahaye, C. Menotti, L. Santos, M. Lewenstein, and T. Pfau, Rep. Prog. Phys. **72**, 126401 (2009).
[20] S. S. Natu, L. Campanello, and S. Das Sarma, Phys. Rev. A **90**, 043617 (2014).
[21] R. M. Wilson and S. Natu, Phys. Rev. A **93**, 053606 (2016).
[22] Y. Cai, M. Rosenkranz, Z. Lei, and W. Bao, Phys. Rev. A **82**, 043623 (2010).
[23] L. Santos, G. V. Shlyapnikov, and M. Lewenstein, Phys. Rev. Lett. **90**, 250403 (2003).
[24] L. Chomaz, R. M. Van Bijnen, D. Petter, G. Faraoni, S. Baier, J. H. Becher, M. J. Mark, F. Wächtler, L. Santos, and F. Ferlaino, Nat. Phys. **14**, 442 (2018).
[25] I. Lesanovsky, Phys. Rev. Lett. **106**, 025301 (2011).
[26] E. Sela, M. Punk, and M. Garst, Phys. Rev. B **84**, 085434 (2011).
[27] H. Weimer and H. P. Büchler, Phys. Rev. Lett. **105**, 230403 (2010).
[28] W. Li, C. Ates, and I. Lesanovsky, Phys. Rev. Lett. **110**, 213005 (2013).
[29] C. Ates, B. Olmos, W. Li, and I. Lesanovsky, Phys. Rev. Lett. **109**, 233003 (2012).
[30] M. Saffman, T. G. Walker, and K. Molmer, Rev. Mod. Phys. **82**, 2313 (2010).
[31] N. Henkel, F. Cinti, P. Jain, G. Pupillo, and T. Pohl, Phys. Rev. Lett. **108**, 265301 (2012).
[32] F. Maucher, N. Henkel, M. Saffman, W. Królikowski, S. Skupin, and T. Pohl, Phys. Rev. Lett. **106**, 170401 (2011).
[33] J. Honer, H. Weimer, T. Pfau, and H. P. Büchler, Phys. Rev. Lett. **105**, 160404 (2010).
[34] F. Cinti, P. Jain, M. Boninsegni, A. Micheli, P. Zoller, and G. Pupillo, Phys. Rev. Lett. **105**, 135301 (2010).
[35] N. Henkel, R. Nath, and T. Pohl, Phys. Rev. Lett. **104**, 195302 (2010).
[36] A. Geißler, U. Bissbort, and W. Hofstetter, Phys. Rev. A **98**, 063635 (2018).
[37] A. Lauer, D. Muth, and M. Fleischhauer, New J. Phys. **14**, 095009 (2012).
[38] Y. Chougale and R. Nath, J. Phys. B **49**, 144005 (2016).
[39] C. Gaul, B. J. DeSalvo, J. A. Aman, F. B. Dunning, T. C. Killian, and T. Pohl, Phys. Rev. Lett. **116**, 243001 (2016).
[40] J. B. Balewski, A. T. Krupp, A. Gaj, S. Hofferberth, R. Löw, and T. Pfau, New J. Phys. **16**, 063012 (2014).
[41] M. Płodzień, G. Lochead, J. de Hond, N. J. van Druten, and S. Kokkelmans, Phys. Rev. A **95**, 043606 (2017).
[42] J. Zeiher, R. Van Bijnen, P. Schauß, S. Hild, J. Y. Choi, T. Pohl, I. Bloch, and C. Gross, Nat. Phys. **12**, 1095 (2016).
[43] M. Viteau, M. G. Bason, J. Radogostowicz, N. Malossi, D. Ciampini, O. Morsch, and E. Arimondo, Phys. Rev. Lett. **107**, 060402 (2011).
[44] G. Pupillo, A. Micheli, M. Boninsegni, I. Lesanovsky, and P. Zoller, Phys. Rev. Lett. **104**, 223002 (2010).
[45] Y. Li, A. Geißler, W. Hofstetter, and W. Li, Phys. Rev. A **97**, 023619 (2018).
[46] Y. Y. Jau, A. M. Hankin, T. Keating, I. H. Deutsch, and G. W. Biedermann, Nat. Phys. **12**, 71 (2016).
[47] A. L. Gaunt, T. F. Schmidutz, I. Gotlibovych, R. P. Smith, and Z. Hadzibabic, Phys. Rev. Lett. **110**, 200406 (2013).
[48] N. N. Bogolyubov, J. Phys. USSR **11**, 23 (1947).
[49] Y. Yu, Ann. Phys. **323**, 2367 (2008).
[50] G. Natale, R. M. W. van Bijnen, A. Patscheider, D. Petter, M. J. Mark, L. Chomaz, and F. Ferlaino, Phys. Rev. Lett. **123**, 050402 (2019).
[51] S. M. Roccuzzo and F. Ancilotto, Phys. Rev. A **99**, 041601(R) (2019).
[52] T. Macrì, F. Maucher, F. Cinti, and T. Pohl, Phys. Rev. A **87**, 061602(R) (2013).
[53] I. Seydi, S. H. Abedinpour, R. E. Zillich, R. Asgari, and B. Tanatar, Phys. Rev. A **101**, 013628 (2020).
[54] Z. Tian, S. Y. Chä, and U. R. Fischer, Phys. Rev. A **97**, 063611 (2018).
[55] A. Griesmaier, J. Werner, S. Hensler, J. Stuhler, and T. Pfau, Phys. Rev. Lett. **94**, 160401 (2005).
[56] S. S. Natu and S. Das Sarma, Phys. Rev. A **88**, 031604(R) (2013).
[57] H. J. Maris, Rev. Mod. Phys. **49**, 341 (1977).
[58] C. E. Campbell, E. Krotscheck, and T. Lichtenegger, Phys. Rev. B **91**, 184510 (2015).
[59] K. Beauvois, J. Dawidowski, B. Fåk, H. Godfrin, E. Krotscheck, J. Ollivier, and A. Sultan, Phys. Rev. B **97**, 184520 (2018).
[60] N. Katz, J. Steinhauer, R. Ozeri, and N. Davidson, Phys. Rev. Lett. **89**, 220401 (2002).